Available online at www.sciencedirect.com
SCIENCE DIRECT®
Journal of Nuclear Materials 345 (2005) 136–145
journal of nuclear materials
www.elsevier.com/locate/jnucmat

Microstructural evolution of both as-irradiated and subsequently deformed microstructures of 316 L stainless steel irradiated at 30–160 °C at LANSCE

Bulent H. Sencer [a,*], Stuart A. Maloy [a], Margaret L. Hamilton [b], Frank A. Garner [b]

[a] Los Alamos National Laboratory, Materials Science and Technology (MST-8), Los Alamos, NM 87545, USA
[b] Pacific Northwest National Laboratory, Materials Resources, P.O. Box 999, Richland, WA 99352, USA

Received 22 October 2004; accepted 17 May 2005

Abstract

Specimens of 316 L stainless steel were irradiated to 0.5–10.3 dpa at 30–80 °C with a mixture of 500–800 MeV protons and spallation neutrons at the Los Alamos Neutron Science Center (LANSCE). Tensile test results of irradiated 316 L reported earlier had showed hardening and embrittlement with increasing irradiation dose, with significant irradiation hardening occurring at a dose of as low as 0.5 dpa. Transmission electron microscope (TEM) examination of the irradiated microstructure of 316 L showed black-spot damage (small loops) and somewhat larger faulted Frank loops to produce the hardening. There was an initial decrease in uniform elongation at low dose levels from 49% (unirradiated) to 30% at 1.1 dpa, followed by a second, rather abrupt contribution to ductility loss at higher doses (~2.5 dpa) from 21% at 2.5 dpa to 0.5% at 3 dpa. This second drop in ductility was not accompanied by any visible new or enhanced microstructural development. In the current study additional transmission electron microscope investigation was conducted on both as-irradiated and irradiated plus subsequently deformed 316 L in the vicinity of the second abrupt ductility loss (~2.5 dpa). The steel was observed to deform mainly by twinning and no brittle phases were found in the deformation microstructure. It is proposed that gas accumulation with increasing dpa, especially of hydrogen, may be a contributor to this second abrupt decrease in uniform elongation. Although the retained gas (helium and hydrogen) levels approached ~0.6 at.% total at the highest exposure level, no discernible cavities were observed.

1. Introduction

Austenitic stainless steels are widely used as structural materials in nuclear reactors. In fission spectra of light water-cooled reactors, as well as in fusion neutron spectra and in the mixed proton-spallation neutron spectra generated in accelerator-driven spallation systems, the displacement damage in typical austenitic structural alloys is accompanied by very large generation rates of both helium and hydrogen [1–5]. While helium is generally thought to be an embrittlement problem primarily for higher-temperature applications, hydrogen is usually thought to exert its influence on

* Corresponding author. Tel.: +1 505 664 0766; fax: +1 505 667 8021.
E-mail address: sencer@lanl.gov (B.H. Sencer).

0022-3115/$ - see front matter © 2005 Elsevier B.V. All rights reserved.
doi:10.1016/j.jnucmat.2005.05.005

embrittlement most strongly at lower temperatures, especially when there are high densities of radiation-induced defects available for trapping, concurrent with large amounts of helium.

Since 316 L is not only used in typical fast reactors and light water cooled power reactors but is a tentative candidate material for the fusion reactor and accelerator-driven systems, irradiated austenitic steels have been studied intensively in the last several decades. Typical radiation-induced microstructural features in austenitic stainless steels are dislocation loops, network dislocations, cavities and precipitates [6]. Pronounced changes in microstructural behavior occur in austenitic stainless steels, varying as a function of irradiation temperature. The microstructural response can be roughly divided into two major temperature regimes. In the low-temperature regime (<300 °C), the microstructure of austenitic stainless steels is dominated primarily by small defect clusters (black dots), faulted interstitial dislocation loops, and network dislocations if the latter existed prior to irradiation. The densities of defect clusters and faulted loops are relatively independent of irradiation temperature in this low-temperature regime. Above 300 °C, the radiation-induced microstructure changes from small dislocation loops to a mixture of larger faulted loops, network dislocations that evolve from loops, and also cavities of either bubble and/or void type.

There have been a number of studies [7–12] in which the microstructure of 316 or 304 stainless steel has been studied after irradiation at temperatures below 300 °C, but the microstructures of such steels after irradiation at <80 °C in a mixed proton and spallation neutron environment have only recently been studied.

In a previously published study in this series the results of tensile tests of 304 L and 316 L irradiated at LANSCE showed that significant irradiation hardening occurred at a dose of as low as 0.5 dpa [13]. As shown in Fig. 1, this hardening was accompanied by an initial decrease in uniform elongation at low dose levels, from ~49% in the unirradiated condition to ~30% at 1.1 dpa, followed by a second, rather abrupt loss of ductility at doses ⩾2.5 dpa, ranging from ~21% at 2.5 dpa to ~0.5% at 3 dpa (Fig. 1(a)). This second drop in ductility was not accompanied by any visible new or enhanced microstructural development. The second abrupt change observed in the uniform elongation does not appear as strongly in the total elongation (Fig. 1(b)).

To investigate the origins of irradiation hardening and embrittlement under low-temperature mixed proton and spallation neutron environment, the microstructure of both as-irradiated and as-irradiated but subsequently deformed 316 L were examined by transmission electron microscopy (TEM). Some of the microstructural results presented below for irradiated but undeformed TEM

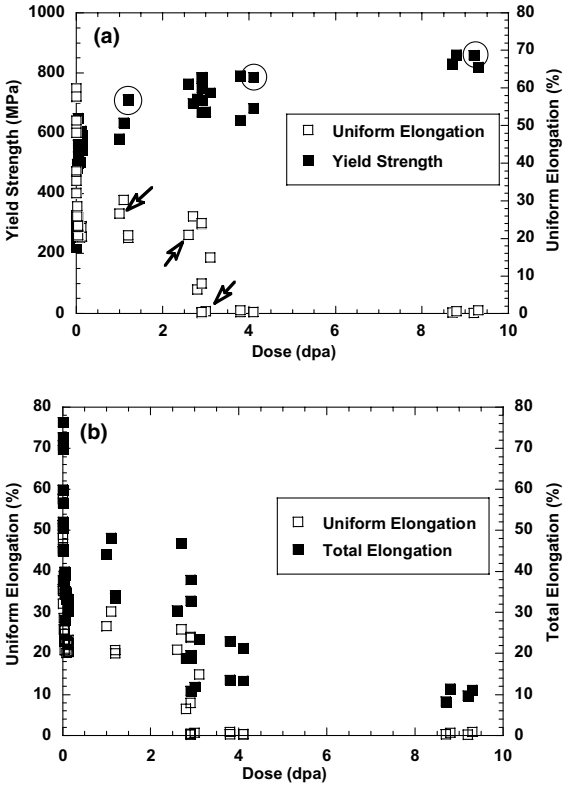

Fig. 1. (a) Graph showing the change in uniform elongation and 0.2% offset yield stress with dose after irradiation in a spallation environment ($T_t = T_{irr} = 50$–160 °C). The specimens for deformation microstructure examined after tensile test are shown by arrows. (b) Graph showing uniform elongation and total elongation as a function of dose.

disks were published previously [14], but additional microscopy results are presented for studies conducted on deformed tensile specimens to ascertain the effect of microstructural alteration, helium and hydrogen on deformation near the dose associated with the second abrupt loss of ductility.

2. Experimental

The chemical composition of 316 L SS employed in this study is summarized in Table 1. Specimens of 316 L SS were electro-discharge-machine (EDM) cut from as-received (annealed) material into either standard 3-mm diameter 0.25 mm thick TEM disks or minitensile specimens (4 mm × 16 mm × 0.25 mm thick, gage dimensions are 1.2 × 5 × 0.25 mm) and received no further heat treatment.

The irradiation was conducted in the LANSCE facility located at Los Alamos National Laboratory. Details of the irradiation were published previously, with all

Table 1
Chemical composition of 316 L used in this study (wt%)

Alloy	C	Si	Mn	Cu	P	S	Mo	Cr	Ni	Fe
316 L	0.019	0.65	1.75	0.26	0.022	0.022	2.57	17.26	12.16	Bal.

specimens irradiated simultaneously at different dpa rates achieved with respect to the proton beam profile [13]. TEM disks and minitensiles were inter-dispersed across the proton beam. The maximum dose achieved in the experiment was about 10.3 dpa, with all doses and gas concentrations determined as described in Refs. [3,5]. The irradiation temperature across the thin tensile and TEM specimens was calculated to vary between 30 and 60 °C, increasing with the dpa rate and its associated proton-induced heating rate. Tensile tests were performed on the minitensiles at 50 and 160 °C at a strain rate of $4 \times 10^{-4}\ s^{-1}$. A summary of the tensile results is shown in Fig. 1 [15].

In addition to the TEM disks examined in the undeformed, as-irradiated condition, 1 mm diameter specimens of post-irradiation deformed material were punched from the gauge area near the heads of previously tested tensile specimens that had been irradiated between 1.1 and 3 dpa. The mechanical properties for both minitensile and shear punch-TEM tests were previously reported by Hamilton et al. [16].

These punched 1.0 mm diameter discs taken from the gauge areas of deformed tensile specimens were then embedded in unirradiated 3 mm diameter discs with 1.0 mm diameter holes at the center. Afterwards, they were jet-polished in a Tenupol with a solution of 5% perchloric acid 95% methanol solution cooled to −20 °C, at 50 V. TEM observation was conducted with a JEOL 2000 FX operated at 200 keV for diffraction-contrast microstructural characterization.

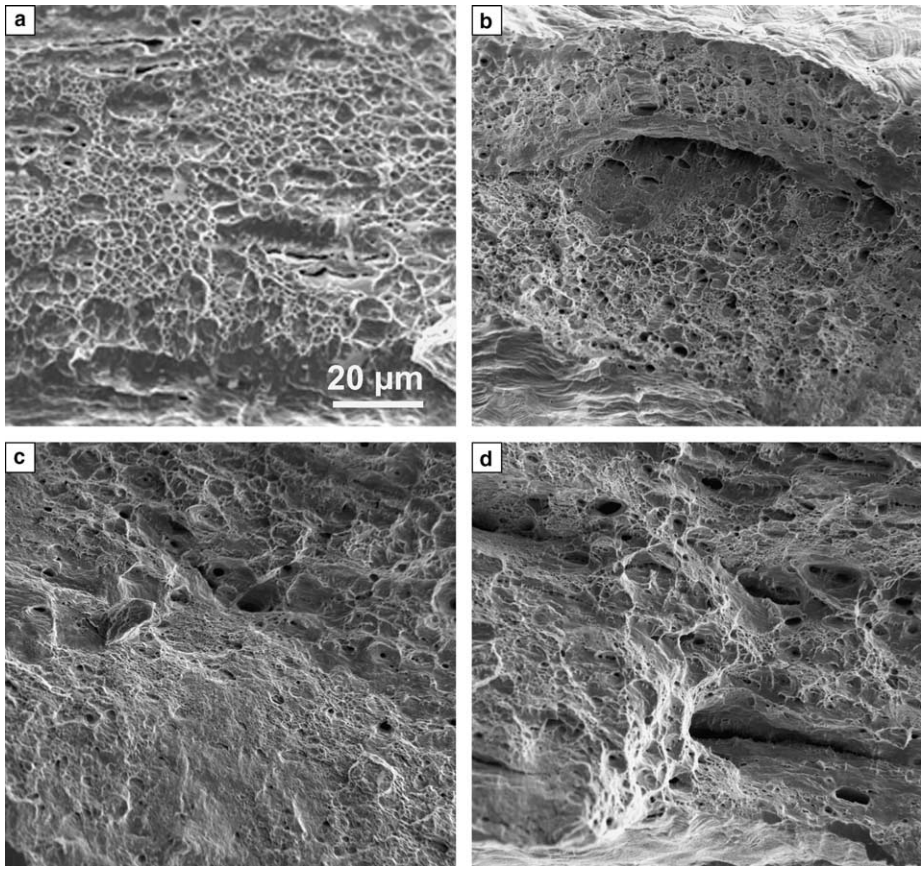

Fig. 2. SEM fractography images of (a) unirradiated 316 L, (b) 1.4 dpa, (c) 4.1 dpa and (d) 9.4 dpa.

3. Results

3.1. SEM fracture surfaces

The fracture surfaces of four 316 L specimens unirradiated and after irradiation to 1.4, 4.1 and 9.4 dpa were examined after tensile testing. The yield stresses measured on these specimens are circled in Fig. 1(a). Four typical fractography images are shown in Fig. 2. Transgranular ductile failure was observed for all specimens. The only subtle difference observed is a decrease in the dimple size with increasing dose. This suggests an increase in void nucleation sites as may be expected with increasing dose.

3.2. Microstructure of unirradiated but deformed 316 L

TEM investigation of unirradiated and deformed 316 L strained to failure (~45% elongation) at room temperature revealed that the deformation mode was primarily via twinning as shown in Fig. 3.

3.3. Microstructure of as-irradiated and undeformed 316 L SS

Proton and spallation neutron irradiation produced a significant change in the microstructure of annealed 316 L stainless steel, as observed in the undeformed TEM disks. Fig. 4 shows black-spot damage (small, unresolved loops $\leqslant$0.5 nm) and somewhat larger faulted Frank loops observed in the weak-beam dark-field (WBDF) imaging condition when observed at 1.4, 3.9 and 10.3 dpa, respectively. A summary of microstructural characteristics obtained from these irradiated specimens is given in Table 2.

Relrod images of faulted Frank loops are shown in Fig. 5, but relrod images can not be used to distinguish between extrinsic or intrinsic stacking faults, i.e. between interstitial or vacancy loops. Loop size distributions and average loop sizes are shown in Figs. 6 and 7, respectively. No resolvable cavity (bubble and/or void) formation was found in the specimens examined up to 10.3 dpa. Resolution limits for such cavities is ~1 nm, allowing the possibility that sub-resolvable vacancy clusters or bubbles might exist.

3.4. Microstructure of irradiated and subsequently deformed 316 L SS

Three specimens produced by punching minitensiles irradiated to 1.1, 2.5 and 3 dpa were prepared to examine the deformation microstructure at exposures near where a sudden drop of uniform elongation occurred (Fig. 1). A TEM image of the deformation microstructure of 316 L strained to failure after irradiation to 1.1 dpa is shown in Fig. 8 together with the corresponding diffraction pattern. Note that the predominant feature of the microstructure is a high density of twins, with a near-total absence of line dislocations. It can also be seen that the narrowest twins are nearly free

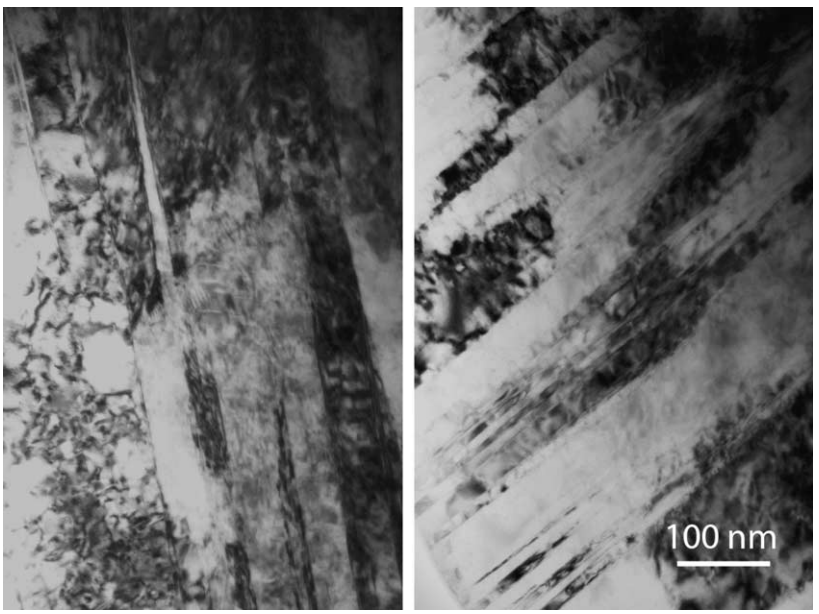

Fig. 3. Bright-field TEM micrographs of deformation twins in unirradiated and deformed sample after tensile testing at room temperature.

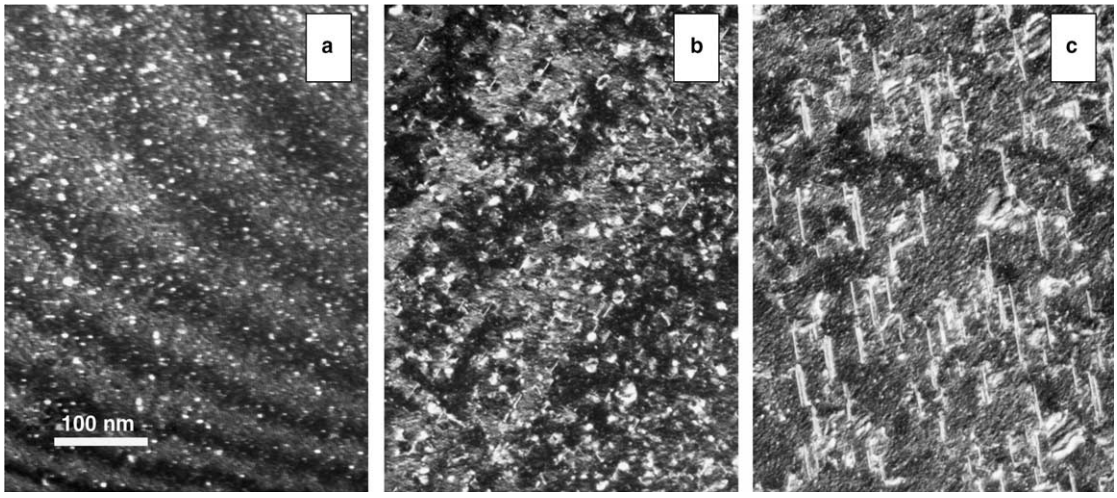

Fig. 4. Weak-beam dark-field $g = 200$ (g/4 g) TEM micrographs of undeformed 316 L, showing black-spot damage and larger faulted Frank loops, taken with the beam direction close to the $\langle 1\ 1\ 0 \rangle$ zone axis, at (a) 1.4, (b) 3.9 and (c) 10.3 dpa.

Table 2
Summary of dislocation loop densities, mean loop diameters, and total dislocation densities for 316 L examined in this study

Alloy	Dose (dpa)	Loop number density (m^{-3})	Mean loop diameter (nm)	Total dislocation density of loops (m^{-2})
316 L	1.4	2.1×10^{22}	4	2.6×10^{14}
316 L	2.5	3×10^{22}	7.1	9.0×10^{14}
316 L	4.1	4.8×10^{22}	10.2	1.54×10^{15}
316 L	10.3	1.9×10^{22}	23.6	1.41×10^{15}

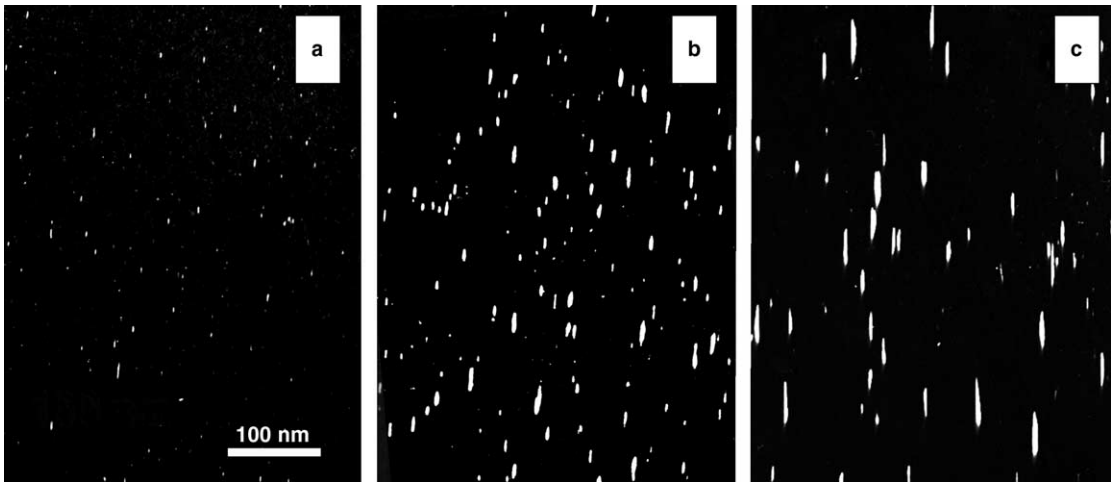

Fig. 5. TEM micrographs of undeformed 316 L showing faulted Frank loops, taken with the beam direction close to the $\langle 1\ 1\ 0 \rangle$ zone axis. (a), (b) and (c) are DF images taken from one of the $\langle 1\ 1\ 1 \rangle$ relrods for specimens at (a) 1.3, (b) 3.9 and (c) 10.3 dpa.

of black spot or loop defects, indicating that most loops were annihilated or unstable after these twins were formed.

Fig. 9 shows a twin in high resolution bright-field and relrod images. The twin zone is nearly free of defects. The twin density and twin width were observed to vary from

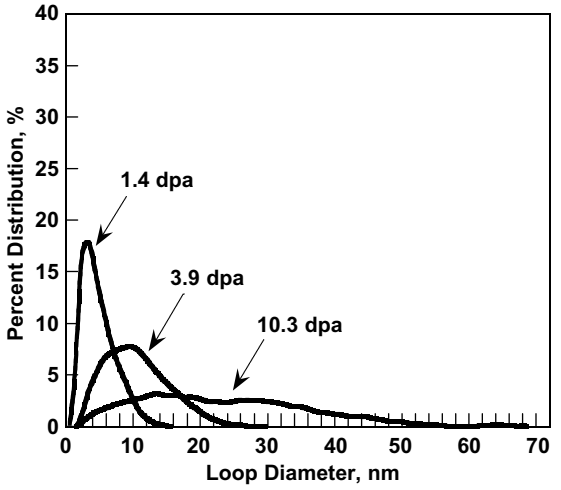

Fig. 6. Loop size distributions as a function of dose, for undeformed 316 L specimens at 1.4 dpa, 3.9 dpa, and 10.3 dpa.

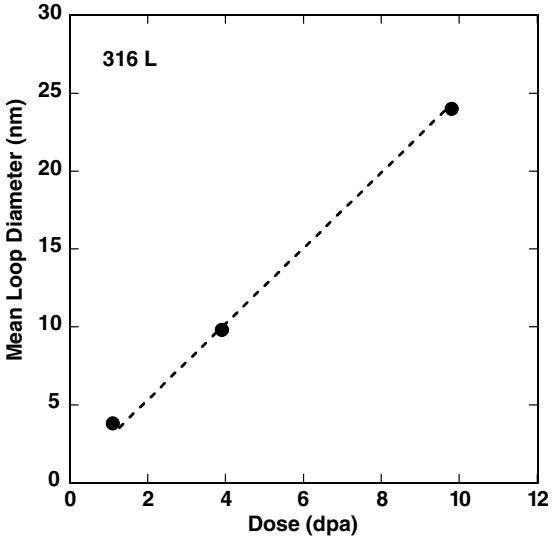

Fig. 7. Mean loop diameter as a function of dose for 316 L stainless steel irradiated at 30–60 °C with a mixed spectra of high-energy protons and spallation neutrons.

grain to grain. The average twin spacing was approximately 0.2–0.3 μm and the width of the twins varied between 20 and 220 nm. Most grains showed primary and secondary twinning on {1 1 1} planes as shown in Figs. 10 and 11. It is obvious from these micrographs that 316 L deforms at room temperature primarily by twinning, independent of the irradiation dose level.

4. Discussion

Combined proton and spallation neutron irradiation at 30–60 °C produced relatively small but significant changes in the microstructure of 316 L when compared to more dramatic microstructural changes usually observed after irradiation at higher temperatures. Black-spot damage was present at all dose levels studied, while larger faulted Frank loops became more numerous as the dose increased. At 0.7 dpa the predominant microstructural feature is unresolvable black-spot damage or small resolvable Frank loops, almost all of which are smaller than 6 nm. Loops grow larger as a function of dose, reaching an average size of ~50 nm at 10.3 dpa. The average loop diameter at 1.4 dpa is smaller by a factor of ten than that at 10.3 dpa. Neither electron diffraction patterns nor stereo-micrographs revealed

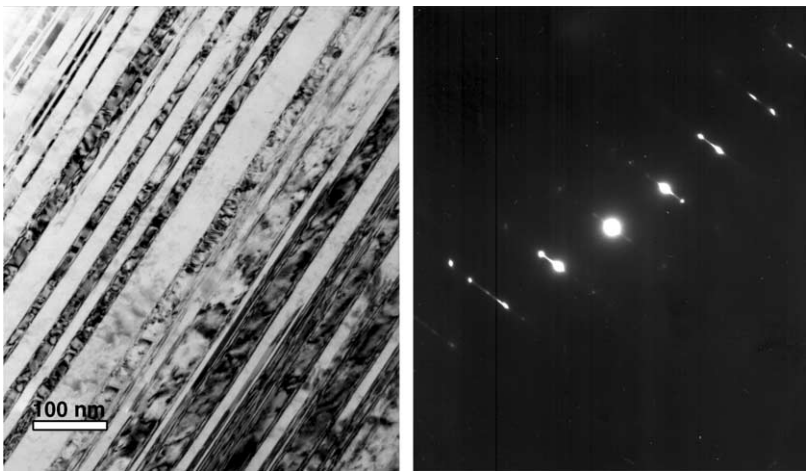

Fig. 8. This image shows twinning in bright-field and the corresponding diffraction pattern of irradiated and subsequently deformed 316 L stainless steel. The irradiation dose is 1.1 dpa with irradiation and test temperatures of 45 and 50 °C, respectively.

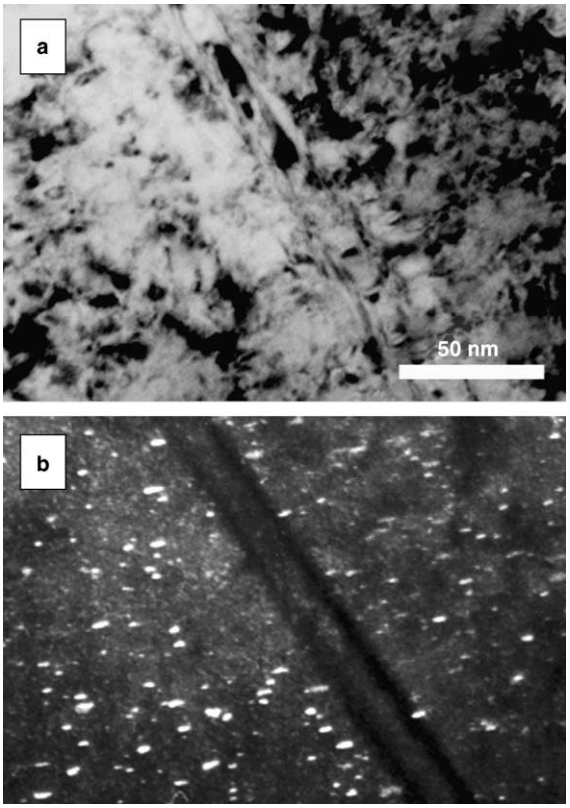

Fig. 9. Microstructure of irradiated and deformed 316 L stainless steel after tensile testing at 20 °C with a strain rate of $4 \times 10^{-4}\,s^{-1}$ after irradiation at 42 °C to 2.5 dpa. The electron micrographs were taken with beam direction close to [0 1 1]. (a) A bright-field image, (b) a dark-field image taken using 1 1 1 streaks arising from the faulted loops.

any evidence of radiation-induced precipitation either in the matrix or at the grain boundaries.

The deformation microstructure of 316 L SS examined between 1.1 and 3 dpa shows twinning as the dominant mode of strain accommodation. Twin formation, a common phenomenon in alloys with low stacking fault energy (SFE), generally reduces ductility and promotes premature failure. The separation of a perfect dislocation into two Shockley partials separated by a layer of stacking fault is energetically favorable in low SFE materials, such as 316 L SS. Twinning is a result of faulting on a succession of layers. Therefore it becomes necessary to have a mechanism whereby the generation of a faulted layer on successive planes is possible. Cottrell and Bilby [17] first proposed a dislocation mechanism for twinning which was later extended by Venables [18]. This mechanism, termed a pole mechanism, requires the dissociation of a perfect dislocation into two segments a glissile Shockley partial, and a sessile segment. The twinning dislocation rotates around a pole whose component Burgers vector is perpendicular to

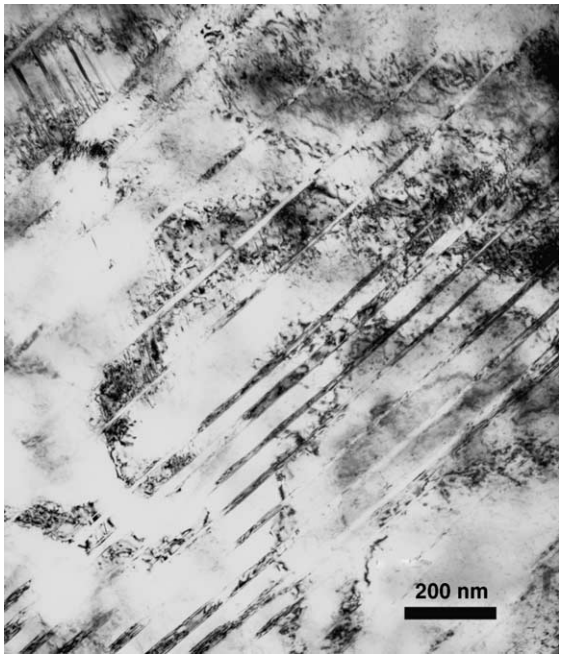

Fig. 10. Bright-field images shows twinning at 2.5 dpa with the irradiation and test temperatures of 42 and 20 °C, respectively.

Fig. 11. Bright-field images shows intersections of two sets of twins at 3 dpa with irradiation and test temperatures of 44 and 50 °C, respectively.

the twin plane and is equal in spacing to the spacing between atomic planes. The sweeping dislocation produces a fault on every successive plane leading to an unfaulted

final structure. The deformation mode can be influenced by the presence of faulted Frank loops and their overall size, density, strain rate and temperature.

As discussed in Ref. [3] the damage-producing spallation process arising from such high-energy particles is much more complex than from the damage process of lower-energy particles. The spallation process involves two primary stages. The first stage involves an intranuclear cascade when the particle enters the nucleus, producing a large number of high-energy secondary particles, including protons, neutrons and sub-nuclear particles. The remaining post-cascade nucleus is now in a highly excited state and undergoes the second stage involving an evaporation event, producing neutrons, alpha particles and more protons, although the latter have a much lower spectrum of energies compared to those produced by the first stage. The recoil of the post-evaporation remaining nucleus is thought to account for the majority of the displaced atoms, although there are contributions from all of the ejected neutrons, protons and alpha particles from both stages. While essentially all helium is produced in the evaporation stage, the hydrogen is produced in roughly equal amounts in both stages. However, the hydrogen produced in the intranuclear cascade is on the order of 100 MeV with large ranges, and a large amount (>60%) of these protons is lost through the surface in specimens of the size relevant to the current experiment. Almost all of the generated helium and a significant fraction of the hydrogen generated during the evaporation event are, however, retained in the specimens. The cross-sections for hydrogen and helium production, as well as dpa production, are known to increase approximately linearly with incident particle energy, such that the gas production to dpa ratios are roughly independent of proton energy spectra as the original 800 MeV protons are down-scattered in energy.

The cross-sections for production of hydrogen are about an order of magnitude greater than those for helium. In this experiment 316 L has retained ~553 appm helium and ~1555 appm hydrogen at ~4 dpa, and ~1720 appm helium and ~3910 appm hydrogen at ~10 dpa as determined experimentally [3–5]. The retained helium was found to increase continuously at a rate of ~180 appm/dpa, while the hydrogen retention was twice as high. However, no cavity (bubble and/or void) formation was found in the specimens examined between 0.7 and 10.3 dpa.

It is important to note that, in the current study, the maximum combined gas retention (helium, hydrogen) was ~0.6 at.%, but led to no resolvable cavity formation. However, in another study involving accelerator implantation of gases and increasing helium above 1 at.%, bubbles were formed and grew continuously at 200 °C in 316 LN austenitic steel [10]. After 5 at.% helium implantation bubble lattices were reported [10].

The observed radiation-induced changes in mechanical properties should be explainable in terms of microstructural alterations induced by radiation, and for this study, it is important to calculate whether the hardening observed in the 316 L can be explained in terms of only the microstructural alterations. According to the theory of hardening based on a hard-sphere model (Orowan model), the change in yield stress change due to dislocation loops, $\Delta\sigma_y$ is expressed by, $\Delta\sigma_y = M\alpha\mu b(Nd)^{1/2}$ where M = Taylor factor, α = barrier strength of obstacles, μ = shear modulus, b = Burgers vector, N = density of dislocation loops, and d = mean diameter of dislocation loops [19]. The α values required to produce the observed hardening were calculated from the yield stresses, loop densities, and loop sizes. From these microstructural data and α value of 0.3–0.5 was calculated between ~4 and 10 dpa [14]. This value is close to estimates obtained by others [20]. Nothing can be definitively concluded about the contribution of the accumulating gas atoms to the hardening and concurrent ductility loss, but the observation that the Frank-loop hardening contribution quickly saturates with increasing exposure, as does the yield strength, tends to argue that the increasing gas (in either atomistic form or in sub-resolvable clusters) is not contributing significantly to the hardening up to 10.3 dpa.

However, the uniform elongation of 316 L initially falls with increasing dose and appears to be saturating at ~21% at ~2.5 dpa, but then drops precipitously to ~0.5% and never recovers as the dpa increases thereafter [15]. A similar behavior was observed in 304 L. In each alloy it appears that accumulating gas contributes to the strong loss in elongation, even though there is no resolvable cavity microstructure, thus requiring the gas to exert its influence while in atomistic or sub-resolvable cavity form.

Existence of a high quantity of gas (hydrogen and helium) in metals is known to have deleterious effect on ductility especially for hydrogen at low temperature [21]. Helium embrittlement is generally considered to be a high-temperature (>350 °C) phenomenon. Hydrogen, however, has been assumed to diffuse away, out of the alloy, at high temperatures. Therefore, the potentially deleterious effect of hydrogen on mechanical properties has also been considered to be very minor [22]. At low-temperatures (<100 °C) helium becomes almost immobile, while hydrogen is thought still to have some mobility. The deleterious effects of hydrogen on the mechanical properties of many unirradiated materials have long been recognized, although the mechanism(s) of hydrogen embrittlement have been the subject of much debate [23]. Of the many suggestions, three mechanisms appear to be viable: stress-induced hydride formation and cleavage [24], hydrogen-enhanced localized plasticity [25–27], and hydrogen-induced decohesion [26]. The effect of hydrogen on deformation and fracture

processes has generally been studied using the in situ environmental-cell TEM deformation technique. In nickel [25], high-purity aluminum [26] and high-strength aluminum (7050, 7075) alloys [27], solute hydrogen reduces the flow stress and enhances dislocation activity. High hydrogen concentrations in the stress field ahead of the crack produce highly localized ductile fracture (hydrogen-enhanced localized plasticity). The effects of hydrogen on the tensile and toughness properties of HT-9 have been investigated after cathodic charging. Charging at 0.003 A/cm^2 for 90 min reduced the tensile ductility by 63%, and changed the fracture mode from dimpled rupture to a combination of intergranular cracking in 12Cr–1Mo steel [28]. Further studies were performed on 12Cr–1Mo steel charged with hydrogen for times ranging from 10 to 150 min [29]. In the uncharged condition, the specimens failed by intragranular rupture and prominent secondary cracking along the prior austenite grain boundaries. Tensile ductility decreased 33% at 0.003 A/cm^2, 15 min, and the degree of secondary cracking increased. At 0.003 A/cm^2 for 150 min, the ductility decreased further and the fracture mode changed to intergranular. Auger analysis indicated that there was a segregation of phosphorous and carbide-forming elements Cr, Mo, W to the prior austenite grain boundaries. For more severe charging levels, the ductility loss was greater, and the fracture mode changed from intragranular rupture to classical intergranular.

In LANSCE, helium is generated with a rate of 180 appm/dpa and hydrogen is retained at ~360 appm/dpa [4]. Therefore, it appears likely that gas accumulation with the increasing dpa especially that of hydrogen may be a major contributor to the abrupt decrease in uniform elongation.

Recently it has been shown that hydrogen tends to be retained at rather high levels when coexisting with rather high levels of helium, especially when cavities are formed [4,30]. Perhaps the high cogeneration of helium and hydrogen potentiates the effect of hydrogen. Remember, however, that resolvable cavities were not observed in these specimens, requiring that such a synergistic effect of helium and hydrogen must work at sub-resolvable cavity levels.

The second abrupt change observed in the uniform elongation probably arises from hydrogen's influence on flow localization, probably because it is more severely affected by the lack of work hardening, as evidenced in the strain before necking. The fact that such an abrupt drop does not appear as strongly in the total elongation (Fig. 1(b))implies that hydrogen's effect is to pin the irradiation-produced microstructure, but once the dislocations are free and mobile, hydrogen's influence is not as abrupt with dose, even though it obviously contributes to the ductility loss.

Also an alternative explanation is that the severe loss of uniform elongation is associated with both irradiation hardening and flow softening. Recent modeling work [31] has shown that constitutive relations for irradiated metals can sometimes be modeled as, $\sigma_{fl} = \sigma_y - C\epsilon_S + k(\epsilon - \epsilon_S)^n$, where σ_{fl} is the flow stress, σ_y the yield stress, C a strain softening coefficient to describe softening over a strain range ϵ_S, k a strain hardening coefficient, ϵ is total plastic strain and n a strain hardening exponent. Irradiation hardening (increases in σ_y) and strain softening (increase in C) lead to significant decreases in uniform elongation. The twins in irradiated material appear near devoid of black spots and loops suggest that localized strain softening may be occurring.

5. Conclusions

Proton and spallation neutron irradiation at 30–60 °C induced the formation of both black-spot damage (small loops) and larger faulted Frank loops in 316 L stainless steel. Faulted Frank-loop sizes increased with increasing dose, while the saturation density was reached rather quickly. In spite of the large levels of helium and hydrogen retention, no cavities were found even at the highest dose examined. Using classic barrier hardening models, the black spot and faulted loop population can account by themselves for the observed increase in yield stress in 316 L. High levels of accumulated helium and hydrogen do not appear to yield a significant contribution to yield stress, but do seem to severely impact the ultimate elongation, especially above 2.5 dpa.

The deformation microstructure of unirradiated 316 L is dominated by twinning which is the dominant mode of strain accommodation. Radiation at 30–60 °C does not appear to alter the twinning-dominated deformation behavior. The radiation-induced loss of ductility observed in 316 L is thought to be due primarily to radiation-induced hardening by faulted Frank loops, and second, to gas accumulation at higher doses, especially hydrogen.

Acknowledgements

This work was supported by the US Department of Energy under the Accelerator Production of Tritium Program, managed by Los Alamos National Laboratory. Battelle Memorial Institute operates Pacific Northwest National Laboratory for USDOE.

References

[1] F.A. Garner, L.R. Greenwood, Radiat. Eff. Def. 144 (1998) 251.
[2] L.R. Greenwood, F.A. Garner, J. Nucl. Mater. 233–237 (1996) 1530.
[3] F.A. Garner, B.M. Oliver, L.R. Greenwood, M.R. James, P.D. Ferguson, S.A. Maloy, W.F. Sommer, J. Nucl. Mater. 296 (2001) 66.

[4] F.A. Garner, B.M. Oliver, L.R. Greenwood, D.J. Edwards, S.M. Bruemmer, M.L. Grossbeck, in: 10th International Conference on Environmental Degradation of Materials in Nuclear Power Systems Water Reactors, 2001, issued on CD format.
[5] B.M. Oliver, F.A. Garner, S.A. Maloy, W.F. Sommer, P.D. Ferguson, M.R. James, in: 20th International ASTM Symposium on Effects of Radiation on Materials, Williamsburg, Virginia, 6–8 June 2000, p. 612.
[6] S.J. Zinkle, P.J. Maziasz, R.E. Stoller, J. Nucl. Mater. 206 (1993) 266.
[7] N. Yoshida, J. Nucl. Mater. 174 (1990) 220.
[8] P.J. Maziasz, J. Nucl. Mater. 191–194 (1992) 701.
[9] J.I. Cole, S.M. Bruemmer, J. Nucl. Mater. 225 (1995) 53.
[10] E.H. Lee, J.D. Hunn, T.S. Byun, L.K. Mansur, J. Nucl. Mater. 280 (2000) 18.
[11] N. Hashimoto, S.J. Zinkle, A.F. Rowcliffe, J.P. Robertson, S. Jitsukawa, J. Nucl. Mater. 283–287 (2000) 446.
[12] Y. Dai, X. Jia, J.C. Chen, W.F. Sommer, M. Victoria, G.S. Bauer, J. Nucl. Mater. 296 (2001) 174.
[13] S.A. Maloy, W.F. Sommer, R.D. Brown, J.E. Roberts, J. Eddleman, E. Zimmerman, G. Willcutt,Tsadasc, in: M.S. Weshler, L.K. Mansur, C.L. Snead, W.F. Sommer (Eds.), Proceedings of Symposium on Materials for Spallation Neutron Sources, TMS, Warrendale, PA, 1998, p. 35.
[14] B.H. Sencer, F.A. Garner, G.M. Bond, S.A. Maloy, M.R. James, W.F. Sommer, in: 20th International ASTM Symposium on Effects of Radiation on Materials, ASTM STP 1405, p. 588.
[15] S.A. Maloy, M.R.. James, G. Willcutt, W.F. Sommer, M. Sokolov, L.L. Snead, M.L. Hamilton, F.A. Garner, J. Nucl. Mater. 296 (2001) 119.
[16] M.L. Hamilton, F.A. Garner, M.B. Toloczko, S.A. Maloy, W.F. Sommer, M.R. James, P.D. Ferguson, M.R. Louthan Jr., J. Nucl. Mater. 283–287 (2000) 418.
[17] A.H. Cottrell, B.A. Bilby, Philos. Mag. 43 (1951) 573.
[18] J.A. Venables, Philos. Mag. 6 (1961) 379.
[19] A. Seeger, in: Proceedings of Second UN International Conference on Peaceful Uses of Atomic Energy, vol. 6, Geneva, 1958, p. 250.
[20] G.E. Lucas, J. Nucl. Mater. 206 (1993) 287.
[21] M.R. Louthan Jr., N.C. Iyer, M.J. Morgan, Mater. Charact. 43 (1999) 179.
[22] W.J.S. Yang, D.S. Gelles, J.L. Straalsund, R. Bajaj, J. Nucl. Mater. 132 (1985) 249.
[23] H.K. Birnbaum, P. Sofronis, Mater. Sci. Eng. 176 (1994) 191.
[24] S. Gahr, M.L. Grossbeck, H.K. Birnbaum, Acta Metall. 25 (1977) 125.
[25] I.M. Robertson, H.K. Birnbaum, Acta Metall. 34 (1986) 353.
[26] G.M. Bond, I.M. Robertson, H.K. Birnbaum, Acta Metall. 36 (1988) 2193.
[27] G.M. Bond, I.M. Robertson, H.K. Birnbaum, Acta Metall. 35 (1987) 2289.
[28] J.M. Hyzak, W.M. Garrison, Alloy Development for Irradiation Performance, Semiannual progress Report for Period Ending 30 September 1981, DOE/ER- 0045/12, p. 186.
[29] J.M. Hyzak, W.M. Garrison, Alloy Development for Irradiation Performance, Semiannual Progress Report For Period Ending 31 March 1984, DOE/ER-0045/12, p. 401.
[30] L.R. Greenwood, F.A. Garner, B.M. Oliver, M.L. Grossbeck, W.G. Wolfer, in: M.L. Grossbeck, T.R. Allen, R.G. Lott, A.S. Kumar, (Eds.), 21st International Symposium, ASTM STP 1447, p. 529.
[31] G.R. Odette, M.Y. He, E.G. Donahue, G.E. Lucas, in: Small Specimen Test Techniques, in: M. Sokolov, J. Landes, G. Lucas (Eds.), ASTM STP 1418, vol. 4, ASTM International, West Conshohocken, PA, 2002, p. 221.